EPJ manuscript No.
(will be inserted by the editor)

Study of hydrogen confined in onion shells

A. L. Frapiccini[1a] and D. M. Mitnik[2]

[1] IFISUR, Universidad Nacional del Sur, CONICET, Departamento de Física - UNS, Av. L. N. Alem 1253, B8000CPB - Bahía Blanca, Argentina.
[2] IAFE, (UBA - CONICET), C1428EGA Buenos Aires, Argentina.

Abstract. In this work we present a theoretical study of the photoionization for atomic hydrogen confined in onion fullerene compared with the bare H atom and the single fullerene case. We obtained the expected confinement resonances for the integrated energy spectrum, finding different trends for the main peak and the first ATI peak integrations. We perform this calculations with a recently developed methodology using Generalized Sturmian Functions to numerically solve the time-dependent Schrödinger equation.

1 Introduction

In recent years, the study of the response to an electromagnetic field of an atom encapsulated in a fullerene cage has been the subject of several theoretical works (see for examples [1, 2]). Examples of situations and phenomena of direct relevance to confined atoms are helium droplets [3], nano-size bubbles formed in liquid helium [4], atoms A encapsulated in hollow cages of carbon based nanomaterials, such as endohedral fullerenes A@C_{60} [5–7], the chemical reactivity and chemical valence of atoms [8], the reversible storage of ions in certain solids [9, 10], the appearance of helium bubbles under high pressure in the walls of nuclear reactors [11], and ESR, NMR and magnetic moments of compressed atoms [12], etc. Confined atoms are also very close in principle to the concepts underpinning confinement within "quantum dots" [13–15]. Thus, the concept of a confined atom provides insight into various problems of interdisciplinary significance.

A special case of the fullerene is that of the so-called fullerene onions or buckyonions, which consists of hollow carbon cages in which smaller buckyballs are encapsulated into larger ones (Cn@Cm@...). [16–18]. Interestingly, fullerene onions have been detected in the interstellar medium [19, 20], and were produced by synthesis by Ugarte in 1992 [21]. Although confinement resonances in photoionization spectra of A@C_60's have been studied extensively, little is known about confinement resonances in photoionization spectra of atoms confined in fullerene onions.

The model-potential method was a first step to study and qualitatively predict the confining effects of the cage on the spectral and dynamic properties of the atom. The external environment imposed by the fullerene cage can, in many instances, be described quite well by a simple, local, spherically symmetric, attractive cage potential that is generally taken to be of constant depth in the region of the fullerene. Photoionization of atoms which are influenced by this model potentials has been treated using a number of methodologies, such as Hartree-Fock (HF) [1, 22], random-phase approximation (RPA) [1, 23, 24], time-dependent close-coupling (TDCC) [25, 26], R-matrix [27], and matrix iterative method [28].

In a previous work [29], we proposed to use the Generalized Sturmian Functions (GSF) [30] to numerically solve the time-dependent Schrödinger equation of a caged atom interacting with a laser pulse. The adaptability of the GSF is key in this methodology, since we can use exponential decaying (real) Sturmians to solve the time-dependent portion of the problem, and the outgoing wave (complex) Sturmians for the time-independent term. To propagate the time-dependent wave packet during the interaction with the pulse, we use and explicit integrating scheme known as Arnoldi [31, 32], which is a Krylov subspace method. The methodology presented proved to be a useful approach to solve the TDSE avoiding the use of integrals to obtain ionization amplitudes.

Following this work, we propose to use the GSF methodology to study the photoionization of atomic H encapsulated in fullerene onions. We compare the photoionization spectra for the H@C_{60} and H@C_{240} with the onion structure H@C_{60}@C_{240}, analyzing the confinement resonances for the main peak and the first ATI peak separately.

In Sec.2 we present an outline of the methodology to extract the ionization amplitude and the spectral density for a one-electron atomic system. In Sec. 3 we present results for the study of avoided crossings due to the change in the depth of the spherical well model potential used to represent the effect of the fullerene. To our knowledge, no research on the avoided crossing due to two spherical wells has been done before. We also present results for the photoinization of the caged H, and concentrate the in the analysis of the confinement resonances in the photoion-

[a] *e-mail: afrapic@uns.edu.ar*

ization spectra, calculating separately the contribution for the main (L=1) peak and first ATI (L=0) peak.

Atomic units are used throughout unless otherwise indicated.

2 Theory

2.1 Time-independent Schrödinger equation: bound states

The effect of the confinement of the hydrogen atom by a fullerene shell is modeled by a spherical well

$$V_w^{(i)}(r) = \begin{cases} -U_0^{(i)} & \text{if} \quad r_c^{(i)} \le r \le r_c^{(i)} + \Delta^{(i)} \\ 0 & \text{otherwise} \end{cases} \tag{1}$$

where $r_c^{(i)}$ is the inner radius of the well and $\Delta^{(i)}$ its thickness. In the case of the onion shells, the potential can be written as

$$V_w(r) = \sum_{i=1}^{n} V_w^{(i)}(r) \tag{2}$$

for an n-walled fullerene cage. For our study we will restrict the potential to $n = 2$.

The bound states of the caged atom are obtained by solving the time-independent Schrödinger equation (TISE)

$$[H_0 + V_w]\,\Psi_\nu(\mathbf{r}) = E_\nu \Psi_\nu(\mathbf{r}) \tag{3}$$

with

$$H_0 = T - \frac{Z}{r} \tag{4}$$

where T is the operator of the kinetic energy and Z is the atomic charge.

To solve the TISE Eq. (3) we expand the wave function in spherical coordinates, and use generalized Sturmian Functions (GSF) [30,33]

$$\Psi_\nu(\mathbf{r}) = \sum_{jlm} a_{jl}^{\nu} \frac{S_{jl}(r)}{r} Y_l^m(\widehat{\mathbf{r}}). \tag{5}$$

The generalized eigenvalue problem to solve is

$$[\mathbf{H_0} + \mathbf{V_w}]\,\mathbf{a}_l^\nu = E_{\nu,l}\mathbf{B}\mathbf{a}_l^\nu \tag{6}$$

for each angular momemtum l and $m = 0$. All matrices are real and symmetric, and the overlap term is also positive definite. The size of the matrices depend on the number N_{max} of GSF in the expansion (5), so the dimension of the matrices will be $N_{max} \times N_{max}$.

2.2 Time-dependent Schrödinger equation: photoionization

We write the time-dependent Schrödinger equation (TDSE) for a two particle system interacting with an external field in the form

$$\imath \frac{\partial}{\partial t}\Psi(\mathbf{r},t) = H(\mathbf{r},t)\Psi(\mathbf{r},t) \tag{7}$$

where the Hamiltonian can be written as

$$H(\mathbf{r},t) = H_0 + V_w + H_{int} \tag{8}$$

with $H_0 + V_w$ the unperturbed Hamiltonian, and H_{int} the interaction with the field. The interaction with the field of an electromagnetic pulse of finite duration is

$$H_{int} = \begin{cases} f(\mathbf{r},t) & \text{for} \quad t_0 \le t \le t_{final} \\ 0 & \text{for} \quad t > t_{final} \end{cases} \tag{9}$$

with $\mathbf{r}$ being the electronic coordinates.

The interaction with the pulse, within the dipole approximation, is written using the velocity gauge, and we consider here linear polarization in the $\widehat{\mathbf{z}}$ axis, thus

$$H_{int}(\mathbf{r},t) = -\imath \mathbf{A}(t)\cdot\nabla_{\mathbf{r}} = -\imath |\mathbf{A}(t)| \frac{\partial}{\partial z} \tag{10}$$

For a photon energy ω and a pulse of duration τ we write

$$|\mathbf{A}(t)| = A_0 g(\omega,t)\sin(\omega t) \quad \text{for} \quad t \in [0,\tau]. \tag{11}$$

To solve the TDSE Eq. (7) for $t < t_{final}$ we expand the wave packet in spherical coordinates, and use GSF

$$\Psi(\mathbf{r},t) = \sum_{nl} a_{nl}(t) \frac{S_{nl}(r)}{r} Y_l^0(\widehat{\mathbf{r}}) \tag{12}$$

with $a_{nl}(t)$ the expansion coefficients that depend on time and Y_l^m the spherical harmonics. The set of GSF used to solve the TDSE are real and with exponential decaying behavior at large distances. Details of the methodology involved in solving Eq. (7) with the GSF can be found in a previous article [29].

The differential probability for an electron having the energy E is determined in terms of the spectral density $D(E,t)$:

$$dP = D(E,t)dE, \tag{13}$$

where

$$D(E,t) = \sqrt{2E}\int |C(\mathbf{k})|^2 d\Omega_k \tag{14}$$

with Ω_k denoting the solid angle under which the electron is emitted and the coefficient $C(\mathbf{k})$ the ionization amplitude.

To obtain the coefficients $C(\mathbf{k})$, we find the evolution of the wave packet at $t > t_{final}$, which is equivalent to solve the time-independent Schrödinger equation given by

$$(E - H_0 - V_w)\Psi_{sc}(\mathbf{r}) = \Psi(\mathbf{r}, t_{final}) \tag{15}$$

where $H_0 + V_w$ is the atomic (time-independent) Hamiltonian, Ψ_{sc} is a scattering term with outgoing boundary conditions, and $\Psi(\mathbf{r}, t_{final})$ is the wave packet at the end of the pulse [34].

To see how to extract the coefficients $C(\mathbf{k})$ from Eq. (15), we write this equation by means of the Green's function

$$\Psi_{sc}(\mathbf{r}) = \frac{1}{(E - H_0)}\Psi(\mathbf{r}', t_{final}) = G^+(\mathbf{r},\mathbf{r}')\Psi(\mathbf{r}', t_{final}) \tag{16}$$

Using the properties of the Coulomb Green's function, we can see that the asymptotic form of the scattering function is

$$\Psi_{sc}(\mathbf{r}) \xrightarrow{r\to\infty} -\sqrt{2\pi}C(k\hat{\mathbf{r}})\frac{e^{\imath[kr+(Z/k)\ln 2kr]}}{r} \tag{17}$$

for an electron ejected with momentum $k = \sqrt{2E}$. This means that if the scattering function has the correct (outgoing wave) asymptotic behavior, the ionization amplitude can be extracted from the function at sufficiently large values of the radius r.

3 Results

3.1 Avoided crossing

For this study, we fix the values of $r_c^{(1,2)}$ and $\Delta^{(1,2)}$ and calculate the energy eigenvalues in Eq.(6) for $U_0^{(1,2)}$ in a range from 0 to 2 a.u.. We use the data provided by Xu et al [35] for a fullerene molecule C_{60}, which is $r_c^{(1)} = 5.75$ a.u. and $\Delta^{(1)} = 1.89$ a.u.. The second, outer fullerene is located in place of the C_{240} molecule, with values $r_c^{(2)} = 12.6$ a.u. and $\Delta^{(2)} = 1.9$ a.u. [22].

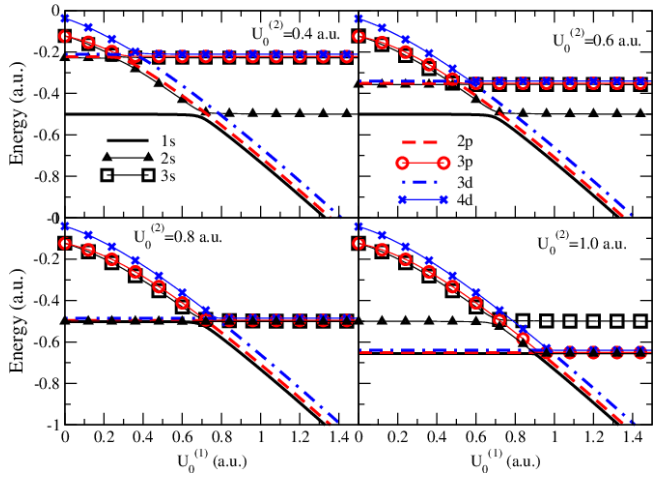

Fig. 1. (Color online) Energies of the H atom confined in two spherical well with $r_c^{(1)} = 5.75$ a.u., $\Delta^{(1)} = 1.89$ a.u., $r_c^{(2)} = 12.6$ a.u. and $\Delta^{(2)} = 1.9$ a.u., as a function of $U_0^{(1)}$ for four different values of $U_0^{(2)}$.

In Fig. 1 we show the results for the firsts s, p and d bound state energy levels. We fixed the value of the second well $U_0^{(2)}$ and plotted the energy as a function of the first well $U_0^{(1)}$. We can see here how the energies behave as the depth of the second well is increased. The first we can notice is that, unlike in the case of a single fullerene cage, we have avoided crossings in the p and d levels. We also observe that the $1s-2s$ crossing remains unchanged until the depth of the second well reaches a value of $U_0^{(2)} \approx$ 0.8 a.u., and then this crossing starts to 'move' to higher values of $U_0^{(1)}$.

In Fig. 2 we can see the radial probability density $\int r^2|\Psi_\nu(\mathbf{r})|^2 d\Omega_r$ for the $1s$, $2s$ and $3s$ states in the vicinity of the avoided crossings. In the top panel in Fig. 2, for $U_0^{(2)} = 0.6$ a.u., there is a 'mirror collapse' between the $2s-3s$ wave functions first and then between the $1s-2s$. As the depth of the second well is increased, for $U_0^{(2)} = 0.8$ a.u. in the center panel in Fig. 2 , the 'mirror collapse' occurs only between the $1s-3s$ levels, while the $2s$ wave function remains unchanged. For $U_0^{(2)} = 1.0$ a.u. in the bottom panel in Fig. 2 we go back to the same ordering as before, $2s-3s$ crossing and then $1s-2s$ crossing. We can also see how, for the first two plots (up to $u_0^{(2)} = 0.8$), we always start with the $1s$ state in the Coulomb well, the $2s$ state in the second fullerene well and the $3s$ state in the first fullerene well. For higher values of $U_0^{(2)}$, the $1s$ and $2s$ are exchanged and now then$1s$ starts in the second well while the $2s$ starts in the Coulomb well.

In Fig. 3 we plotted the radial probability density for the $2p$ and $3p$ states near the avoided crossings for the same cases as the s states. We can see here how, for lower values of $U_0^{(1)}$, the $2p$ state is always located in the second fullerene well, while the $3p$ is in the first fullerene well. As the depth of the first well increases, we observe the mirror collapse between these bound states. It is also observed how the energy crossing for the $2p-3p$ levels 'follows' first that of the $2s-3s$ levels, and after $U_0^{(2)} = 0.8$ follows that of the $1s-2s$ levels.

The avoided crossing phenomena is a mechanism for the state energy reordering, manifested by the energy level repulsion: neighboring energy levels with the same symmetry do not cross each other, but rather come close and repel each other in an avoided crossing. An additional indicator of the external effects resides in the informational character. In information theory, entropy is a measure of the uncertainty associated with a random variable.

In this field, the term usually refers to the Shannon entropy, which measures the expected value of the information contained in a message, usually in units such as bits, i.e., it is a measure of the average information content that is missing when the value of the random variable is unknown.

The Shannon information entropy of one-normalized electron density in the coordinate space [36] is defined as

$$S_r = \int \rho(\mathbf{r}) \ln\left[\rho(\mathbf{r})\right] d\mathbf{r} \tag{18}$$

where the electron atomic density is defined as

$$\rho(\mathbf{r}) = |\Psi_\nu(\mathbf{r})|^2 \tag{19}$$

This quantity is an information measure of the spatial delocalization of the electronic cloud. So, it gives the uncertainty of the localization of the electron. The lower this quantity, the more concentrated the wave function of the state, the smaller the uncertainty, and the higher the accuracy in predicting the localization of the electron.

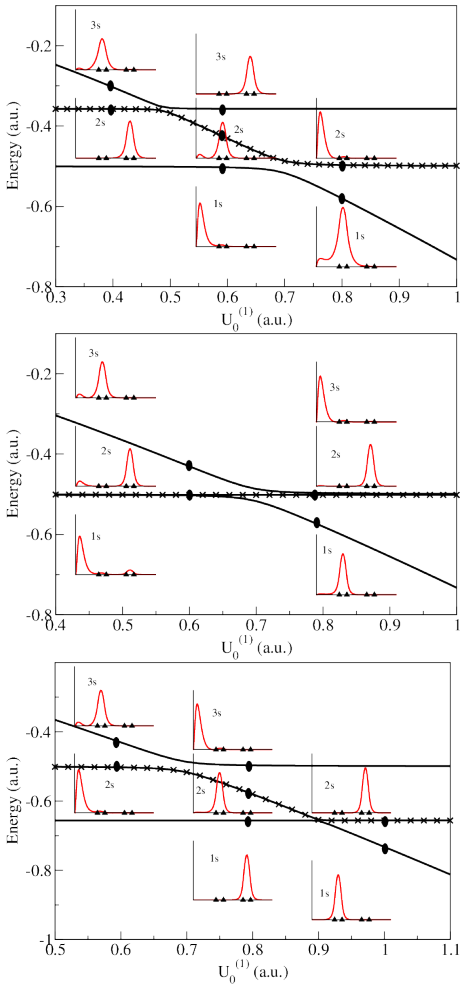

Fig. 2. (Color online) Radial $s-$state probability of the H atom confined in two spherical well with $r_c^{(1)} = 5.75$ a.u., $\Delta^{(1)} = 1.89$ a.u., $r_c^{(2)} = 12.6$ a.u. and $\Delta^{(2)} = 1.9$ a.u. near the energy crossing for $U_0^{(2)} = 0.6$ (top), $U_0^{(2)} = 0.8$ (center) and $U_0^{(2)} = 1.0$ (bottom).

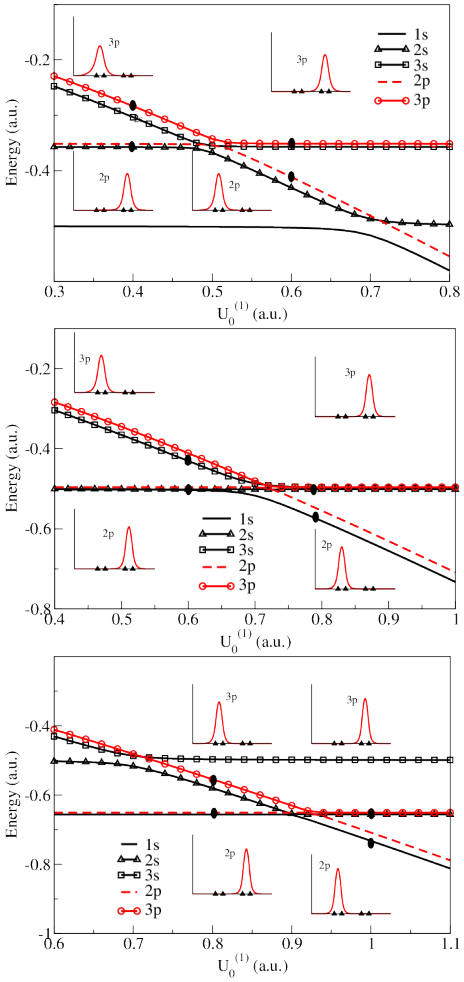

Fig. 3. (Color online) Radial $p-$state probability of the H atom confined in two spherical well with $r_c^{(1)} = 5.75$ a.u., $\Delta^{(1)} = 1.89$ a.u., $r_c^{(2)} = 12.6$ a.u. and $\Delta^{(2)} = 1.9$ a.u. near the energy crossing for $U_0^{(2)} = 0.6$ (top), $U_0^{(2)} = 0.8$ (center) and $U_0^{(2)} = 1.0$ (bottom).

The variation of the Shannon entropy of states with an external potential strength may lead to gaining a deeper physical insight into the dynamics of the system through the avoided crossing region [37].

In Fig. 4 is shown the Shannon information entropy as a function of the first fullerene cage strength for two different values of the outer fullerene cage depth. The same energy levels as in Fig. 1 are plotted. We can see here how the states exchange their informational properties as they go through an avoided crossing.

3.2 Confinement resonances in photoionization

We now turn to the study of the photoionization of the confined atoms, using the methodology described in Sec.2.2. The interaction with the pulse is as described in Eq. 11 with a sine square envelope $g(\omega, t) = \sin\left(\frac{\pi}{\tau}t\right)^2$ with a total duration of $\tau = 2\pi n_c/\omega$, where n_c is an integer giving the number of optical cycles.

We consider photoionization from initial state $1s$. The values for $r_c^{(1)}, r_c^{(2)}, \Delta^{(1)}$ and $\Delta^{(2)}$ are the same as in the previous section, and for the the C_{60} cage, we use the parameters of the model potential found in [35,38]: $U_0 = 8.22$ eV, and for the C_{240} [22]: $U_0 = 10$ eV.

In all the calculations presented now the peak intensity 5×10^{14} W/cm^2 and $n_c = 16$ optical cycles. All the calculations shown in this section were performed using $N_{max} = 300$ and $l_{max} = 10$, and the size of the Krylov space was $n_{Krylov} = 30$, with a fixed time step of $\delta t = 0.03$.

As a first test we performed calculations for photon energies of $\omega = 0.7$ and 0.9 a.u.. The endohedral atoms H@C_{60} and H@C_{60}@C_{240} were compared to the bare H atom.

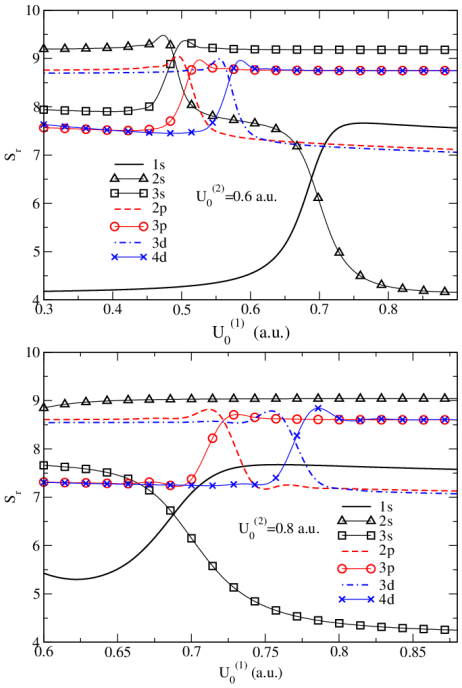

Fig. 4. (Color online) Shannon entropy of the H atom confined in two spherical well with $r_c^{(1)} = 5.75$ a.u., $\Delta^{(1)} = 1.89$ a.u., $r_c^{(2)} = 12.6$ a.u. and $\Delta^{(2)} = 1.9$ a.u. for $U_0^{(2)} = 0.6$ (top) and $U_0^{(2)} = 0.8$ (bottom).

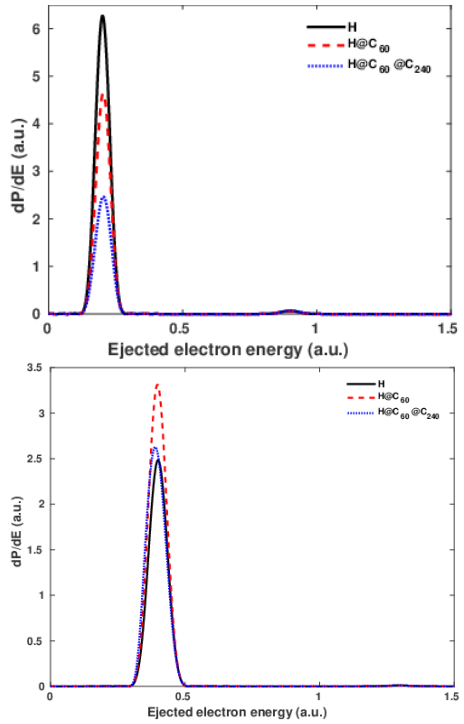

Fig. 5. (Color online) Energy spectrum of the ejected electron for photon energies of $\omega = 0.7$ (top) and 0.9 (bottom) a.u., for the confined and bare H atoms.

The results for the ejected electron energy spectrum are shown in Fig. 5. It is observed here how the intensity of the line is affected by the presence of the cage(s). In the case of $\omega = 0.7$ a.u. for example, we see that the endohedral atom H@C_{60} has a lower intensity than that of the H atom, as well as the H@C_{60}@C_{240} . On the other hand, for $\omega = 0.9$, both intensities are higher than that of the H.

This oscillations in intensity of the spectrum as a function of the photon (photoelectron) energy is due to the 'confinement resonances'. As discussed by Connerade et al [39], they studied the origin and properties of confinement resonances considering hydrogenic ions placed at the centre of a spherical shell as in Eq. (1) for a single well. They assume that the resonances are due to features in final (continuous) electronic states owing to the confinement.

In Fig.(6) we show the results for the integration of the energy spectrum dP/dE around the main peak as a function of the photon energy, for the H@C_{60} and H@C_{60}@C_{240}. We can see here how the presence of the cage(s) affects the intensity of the main peak. The range of photon energy in Fig.(6) corresponds to electrons emitted with energies lower than 3 a.u. in order to ensure that the electron wavelength is larger than the distance between the carbon cage atoms [40]. The addition of the second well for the H@C_{60}@C_{240} increases the number of resonances, as expected.

In Fig.(7) we see the time evolution of the L=1 wave of the radial probability density for the H atom and the

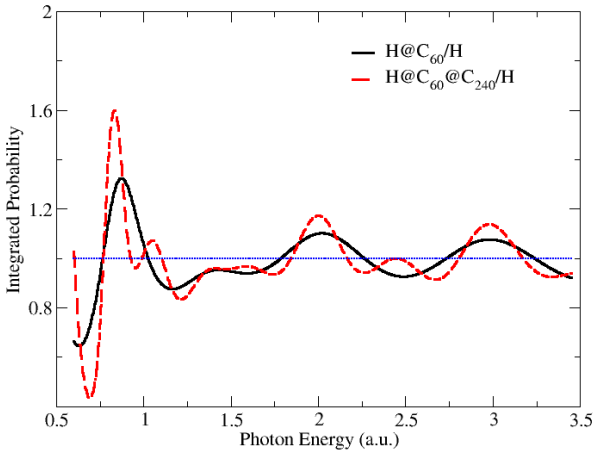

Fig. 6. (Color online) Integrated energy spectrum for the main peak as a function of the photon energy.

encapsulated H@C_{60}. The top panel in Fig.(7) corresponds to a photon energy of $\omega = 0.87$ a.u. near a maximum in Fig. (6) and the bottom panel to $\omega = 1.16$ a.u. near a minimum in Fig.(6). It is clear here the effect of the cage in the constructive (top panel) and destructive (bottom panel) interference in the inner region $0 < r < r_c^1$.

In Fig.(8) we see the time evolution of the L=1 wave of the radial probability density for the H atom and the

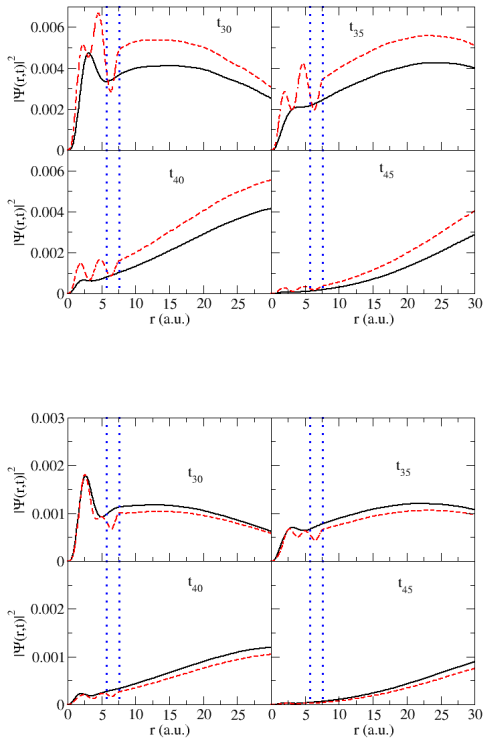

Fig. 7. (Color online) Radial probability density for the L=1 wave for the bare atom H and endohedral H@C_{60} near a maximum resonance (top) and minimum resonance (bottom), for four different time stages during the propagation of the wave packet. Dotted (blue) line shows the location for the C_{60} cage.

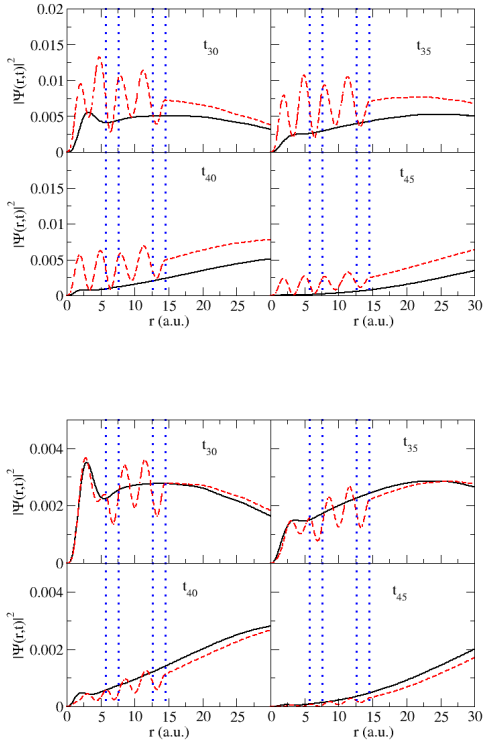

Fig. 8. (Color online) Radial probability density for the L=1 wave for the bare atom H and endohedral H@C_{60}@C_{240} near a maximum resonance (top) and minimum resonance (bottom), for four different time stages during the propagation of the wave packet. Dotted (blue) line shows the location for the C_{60} and C_{240} cages.

encapsulated H@C_{60}@C_{240}. The top panel in Fig.(8) corresponds to a photon energy of $\omega = 0.83$ a.u. near a maximum in Fig. (6) and the bottom panel to $\omega = 0.96$ a.u. near a minimum in Fig.(6). Here we see the effect of the cage in the constructive (top panel) and destructive (bottom panel) interference in the inner region $0 < r < r_c^1$ and also in the region between the two cages.

In [22], the study of multiwalled fullerenes suggested a trend in the confinement oscillations as the atom was encapsulated in larger fullerenes. In Fig. (9) we see how we can draw the same conclusions as in [22] for the integrated main line (P peak), comparing the three cases of H@C_{60}@C_{240}/H with the single walled H@C_{60}/H and H@C_{240}/H. For the caged H atom, in the top panel of Fig. (9) we see how the single walled atoms oscillate around the dotted line (equal to 1), but the H@C_{60}@C_{240} actually seems to oscillate on the H@C_{60} line. To test this, in the bottom panel of Fig.(9) we plotted H@C_{60}@C_{240}/H@C_{60} (red broken line), and it clearly shows a behavior similar to the H@C_{240}/H, except for lower photon energies.

To see if the trend observed for the integrated main line extends to the first ATI peak (S peak), we calculated the same ratios as in Fig. (9) for this peak. If Fig.(10) we can see the same behavior for the ATI peak as for the main line, meaning that the ratio of H@C_{60}@C_{240}/H@C_{60} behaves as the H@C_{240}/H for high photon energies. We see here that the behavior of the P line is not the same as the S line, the location and number of peaks differ. This is mainly due to the intermediate states involved in the two-photon process, which is the primary source of the S peak.

4 Conclusions

We apply an *ab-initio* methodology to solve the time-dependent Schrödinger equation of an atom interacting with an electromagnetic pulse of finite duration. The approach is based on the Generalized Sturmian Functions [29], and their adaptability to define different asymptotic behaviors.

We present an application by studying the influence of the confinement of the H atom in a fullerene cage C_{60} and C_{240} compared with the fullerene onion C_{60}@C_{240}. First we perform a study of the avoided crossing for the onion with a simple spherical well potential to represent the fullerenes. Since we have now two parameters to vary

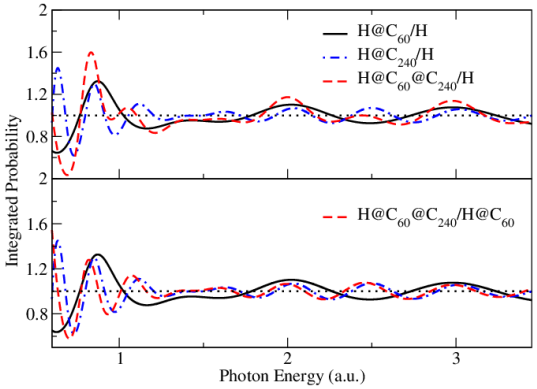

Fig. 9. (Color online)Integrated energy spectrum for the main peak (P peak) as a function of the photon energy. Top panel shows the ratio with respect to the bare H atom, bottom panel shows the single walled H@C_{60} and H@$_{240}$ with respect to H, and the double walled H@C_{60}@C_{240} with respect to H@C_{60}.

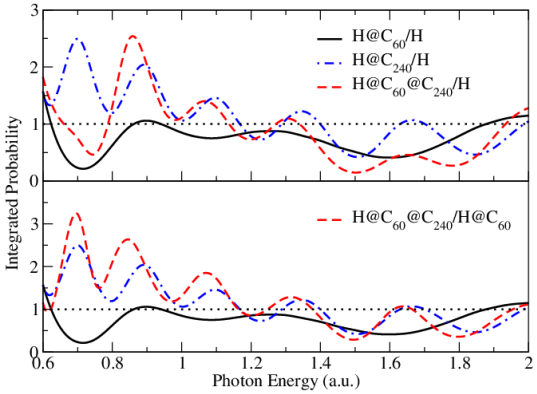

Fig. 10. (Color online) (Color online) Integrated energy spectrum for the first ATI peak (S peak) as a function of the photon energy. Top panel shows the ratio with respect to the bare H atom, bottom panel shows the single walled H@C_{60} and H@$_{240}$ with respect to H, and the double walled H@C_{60}@C_{240} with respect to H@C_{60}.

(the depth of each well), we fix the depth of in the location of the C_{240} cage at several different values, and plot the energy eigenvalues as a function of the depth of the well of the C_{60} . For the cases shown, we observe crossings not only for the s states, as was the case for a single cage, but also crossings in the p and d states. We also show calculations for the Shannon information entropy for the electron density near some of the crossings, which clearly display the exchange of the informational properties as they go through the avoided crossing.

Finally, we calculate the ionization of the bare H and caged atom interacting with an electromagnetic pulse in the range of 0.6 a.u. to 3.4 a.u. of photon energy. We present the results for the energy spectrum integrated around the main peak as a function of the photon energy for the H@C_{60} and H@C_{60}@C_{240} with respect of the bare H atom. We obtained the expected confinement resonances, observing the increase in the number of oscillations in the onion fullerene with respect to the single well fullerene. The plots of the radial probability for the L=1 wave in the vicinity of a maximum of minimum in the energy spectrum show the constructive and destructive interference which give origin to the resonances. The results for the main peak show clearly that at high photon energies, we can separate the effect of the inner C_{60} and outer C_{240} cages for the onion fullerene, which is not the case for lower photon energies.

We perform the same calculations for the first ATI peak, observing the confinement resonances, but at different locations. However, we confirm the same behavior for high photon energies, in which the outer fullerene and inner fullerene effects can be separated.

The calculations performed in encapsulated hydrogen are a useful starting point to study the influence of the onion fullerenes in other atomic systems. The conclusions drawn here are applicable to other atomic systems whose initial state has a similar probability distribution to that of the 1s. While our focus here is to present results for the confined H, other multielectronic atoms could be represented by means of the one-active electron approximation.

Acknowledgments

We acknowledge the support by Grant No. PIP 201301/607 CONICET (Argentina) also thank the support by Grant No. PGI (24/F059) of the Universidad Nacional del Sur.

References

1. V.K. Dolmatov, *Photoionization of Atoms Encaged in Spherical Fullerenes*, Vol. 58 of *Advances in Quantum Chemistry* (Academic Press, 2009)
2. V.K. Dolmatov, A.S. Baltenkov, J.P. Connerade, S.T. Manson, Radiat. Phys. Chem. **70**, 417 (2004)
3. C. Zicovich-Wilson, J.H. Planelles, W. Jaskóalski, International Journal of Quantum Chemistry **50**, 429 (1994)
4. P.L. Goodfriend, Journal of Physics B: Atomic, Molecular and Optical Physics **23**, 1373 (1990)
5. H. Shinohara, Reports on Progress in Physics **63**, 843 (2000)
6. P. Moriarty, Reports on Progress in Physics **64**, 297 (2001)
7. L. Forró, L. Mihály, Reports on Progress in Physics **64**, 649 (2001)
8. J.M. Lawrence, P.S. Riseborough, R.D. Parks, Reports on Progress in Physics **44**, 1 (1981)
9. J.P. Connerade, Journal of Alloys and Compounds **255**, 79 (1997)
10. J.P. Connerade, R. Semaoune, Journal of Physics B: Atomic, Molecular and Optical Physics **33**, 3467 (2000)
11. C.A. Walsh, J. Yuan, L.M. Brown, Philosophical Magazine A: Physics of Condensed Matter, Structure, Defects and Mechanical Properties **80**, 1507 (2000)
12. A.L. Buchachenko, Journal of Physical Chemistry B **105**, 5839 (2001)
13. N.F. Johnson, Journal of Physics: Condensed Matter **7**, 965 (1995)

14. T. Sako, G.H.F. Diercksen, Journal of Physics B: Atomic, Molecular and Optical Physics **36**, 1433 (2003)
15. T. Sako, G.H.F. Diercksen, Journal of Physics B: Atomic, Molecular and Optical Physics **36**, 1681 (2003)
16. B.S. Xu, in *Xinxing Tan Cailiao/ New Carbon Materials* (Elsevier, 2008), Vol. 23, pp. 289–301
17. L. Echegoyen, A. Ortiz, M.N. Chaur, A.J. Palkar, in *Chemistry of Nanocarbons* (John Wiley & Sons, Ltd, Chichester, UK, 2010), pp. 463–483, http://doi.wiley.com/10.1002/9780470660188.ch19
18. J. Bartelmess, S. Giordani, Beilstein Journal of Nanotechnology **5**, 1980 (2014)
19. W.A. de Heer, D. Ugarte, Chemical Physics Letters **207**, 480 (1993)
20. S. Iglesias-Groth, The Astrophysical Journal **608**, L37 (2004)
21. D. Ugarte, Nature **359**, 707 (1992)
22. V.K. Dolmatov, P. Brewer, S.T. Manson, Phys. Rev. A **78**, 013415 (2008)
23. M.Y. Amusia, A.S. Baltenkov, U. Becker, Phys. Rev. A **62**, 012701 (2000)
24. M.Y. Amusia, A.S. Baltenkov, Phys. Rev. A **73**, 062723 (2006)
25. J.A. Ludlow, T.G. Lee, M.S. Pindzola, Phys. Rev. A **81**, 023407 (2010)
26. T. Lee, J.A. Ludlow, M.S. Pindzola, J. Phys. B **45**, 135202 (2012)
27. T.W. Gorczyca, M.F. Hasoglu, S.T. Manson, Physical Review A **86**, 033204 (2012)
28. A.N. Grum-Grzhimailo, E.V. Gryzlova, S.I. Strakhova, J. Phys. B: At. Mol. Opt. Phys. **44**, 235005 (2011)
29. A.L. Frapiccini, G. Gasaneo, D.M. Mitnik, Eur. Phys. J. D **71**, 40 (2017)
30. G. Gasaneo, L.U. Ancarani, D.M. Mitnik, J.M. Randazzo, A.L. Frapiccini, F.D. Colavecchia, *Proceedings of MEST 2012: Exponential Type Orbitals for Molecular Electronic Structure Theory*, Vol. 67 of *Advances in Quantum Chemistry* (Academic Press, 2013)
31. Y. Saad, SIAM J. Numer. Anal. **29**, 209 (1992)
32. A.L. Frapiccini, A. Hamido, S. Schröter, D. Pyke, F. Mota-Furtado, P.F. O'Mahony, J. Madronero, J. Eiglsperger, B. Piraux, Phys. Rev. A **89**, 023418 (2014)
33. A.L. Frapiccini, V.Y. Gonzalez, J.M. Randazzo, F.D. Colavecchia, G. Gasaneo, Int. J. Quantum Chem. **107**, 832 (2007)
34. A. Palacios, C.W. McCurdy, T.N. Rescigno, Phys. Rev. A **76**, 043420 (2007)
35. Y.B. Xu, M.Q. Tan, U. Becker, Phys. Rev. Lett. **76**, 3538 (1996)
36. C.E. Shannon, The Bell System Technical Journal **27**, 379 (1948), 9411012
37. R. González-Férez, J.S. Dehesa, Phys. Rev. Lett. **91**, 113001 (2003)
38. J.P. Connerade, A.V. Solov'yov, Journal of Physics B: Atomic, Molecular and Optical Physics **38**, 807 (2005)
39. J.P. Connerade, V.K. Dolmatov, S.T. Manson, Journal of Physics B: Atomic, Molecular and Optical Physics **33**, 2279 (2000)
40. M.Y. Amusia, A.S. Baltenkov, L.V. Chernysheva, Journal of Physics B: Atomic, Molecular and Optical Physics **41**, 165201 (2008)